J Ther Eng, Vol. 10, No. 2, pp. 273−285, March, 2024

Journal of Thermal Engineering
Web page info: https://jten.yildiz.edu.tr
DOI: 10.18186/thermal.1448547

Journal of Thermal Engineering

Research Article

Thermal stress analysis in pin fin microchannel heat sink

Mohammad Nazirul Syafiqaiman JANI[1], Nawaf H. SAEID[1,*]

[1]*Department of Mechanical Engineering, Universiti Teknologi Brunei, Gadong, BE1410, Brunei*

ARTICLE INFO

Article history
Received: 06 October 2022
Revised: 16 February 2023
Accepted: 02 March 2023

Keywords:
Conjugate Heat Transfer; Numerical Study; Pin-Fin Microchannel; Thermal Stress

ABSTRACT

The conjugate heat transfer and the thermal stresses produced within a pin-fin microchannel heat sink are investigated numerically. The pin-fin microchannel heat sink is subjected to a constant heat flux from the bottom surface and cooled by water flow through the channel across the pin fins. Rectangular cross-section microchannel incorporating one raw of square pin fins are considered. The water flowing through the microchannel at Reynolds number varies from 200 to 800. The heat sink dissipates constant heat flux in the range of 75-175 kW/m^2. The selected materials used for the solid substrate are Copper, Aluminium, Titanium, and Structural steel. The results are presented as contour plots for the temperature, thermal stress, and deformation distribution. It is found that the heat dissipation and the Nusselt number are increased with increasing Reynolds number, increasing the thermal conductivity of the material but remain constant throughout various heat fluxes. Thermal stresses are increased with decreasing Reynolds number, increasing heat flux, and increasing Youngs' Modulus of the substrate material. The total deformation is increased with decreasing Reynolds number, increasing heat flux, and increasing the thermal expansion coefficient of the substrate material.

Cite this article as: Jani MNS, Saeid NH. Thermal stress analysis in pin fin microchannel heat sink. J Ther Eng 2024;10(2):273−285.

INTRODUCTION

Pin fin microchannel heat sinks serve a key role in maintaining the integrity and quality of performance of modern technology electric and electronic hardware by dissipating heat from heated components. Therefore, significant studies have been carried out for better understanding the necessary factors or structural characteristics towards improving the heat dissipation. Initially, conventional smooth microchannels had been utilized to great extents towards dissipating heat from electric components as highlighted in references [1-3]. The effectiveness of adding pin fins to the microchannel structure has been discussed by various studies [4-8] as well as industry usage of the pin fins microchannels by the studies listed in the references [9-14].

Gunnasegaran et al. [15] performed a study examining the effect of varying cross-sectional shapes of the microchannel upon the overall heat transfer performance within the microchannel heat sink, focusing on rectangular, trapezoidal and triangular cross sections. It was concluded that the rectangular cross section displayed the greatest heat transfer performance followed by the trapezoidal and triangular cross sections. Kewalramani et al. [16] found that

***Corresponding author.**
*E-mail address: nawaf.saeid@utb.edu.bn, n_h_saeid@yahoo.com

This paper was recommended for publication in revised form by Editor-in-Chief Ahmet Selim Dalkılıç

maintaining the thickness of the solid substrate within the pin-fin microchannel will prevent potential hotspots to form. Cheng [17] had concluded that utilizing stacked microchannel comprising of passive structures can significantly outperform a conventional singular microchannel. Xie et al. [18] studied the effect of running counter flow configurations within these stacked microchannels and found that these configurations further enhanced the heat transfer characteristics within the overall heat sink. Wang et al. [19] examined the effects of implementing truncated top channels within double-stacked microchannels and concluded the overall rise in performance within the heat sink. When investigating potential additional features to be added within the microchannel walls, it had been highlighted by Ding et al. [20] that cutting ribs and grooves into the side walls of the microchannel could outperform a smooth wall microchannel. This study involved utilizing a singular microchannel heat sink consisting of two parts, an upper wall filled with ribs or grooves and a smooth lower wall. In the efforts of singling out a building material most suitable for constructing a pin-fin microchannel, several studies in the references [16,21-26] had showed preference towards incorporating silicon or copper due to their relatively well established thermal stability, their excellent thermal expansion properties under exposure to heat flux applied, cost effectiveness and general eco-friendly nature. However, it was also concluded that copper stands as a superior choice due to its higher thermal conductivity in comparison to silicon, resulting in it being a better conductive substrate.

In regards to choosing a suitable fluid coolant Grande and Kandlikar [27] highlighted the excellent reliability, low maintenance costs and simple compatibility when utilizing air as the coolant fluid. However, modern technology releasing increasingly greater excess heat to be dissipated. Studies such as those conducted by Luo et al. [28] concluded that the cooling effect due to the air coolant can no longer provide adequate heat extraction. A popular choice that stands is to swap out air with water or nanofluid coolants where these two alternatives have been constantly compared to each other in several studies [29-33]. Park et al. [29] performed numerical analysis on separate pin-fin microchannels with one utilizing nanofluid coolant and the other consisting of water coolants. It was found that nanofluid coolants significantly outperformed water coolants in terms of heat transfer performance. However, due to the difficulty of implementing nanofluids within conventional applications, water coolants have been preferred as the most suitable alternative to replace the traditionally used air coolant.

The flow of the coolant commonly adopts several characteristics within conventional applications and parametric studies regarding the pin-fin microchannel. Ronge et al. [34] had considered the fluid flow to be fully uniform with uniform velocity throughout a pin-fin microchannel. Bhandari and Prajapati [25] had assigned purely atmospheric pressure acting to the fluid outlet of the channel within their study. When conducting their study regarding the modelling of microchannel heat sinks, Saha et al. [35] had applied several assumptions including incompressible fluid flow, negligible heat losses from the arrangement and the flow would be uniformly distributed among the microchannels. These set of assumptions can be standardized within any form of pin-fin microchannel analysis as it considers the ideal conditions.

A crucial element that affects the heat transfer performance of a pin-fin microchannel is the structure or shape of the pin fins. Ronge et al. [34] had compared the heat transfer capabilities of different shaped pin fins: elliptical; circular; square; hexagonal. It was found that at low Reynolds number within laminar flow, circular pin fins showed the best overall thermal performance. In contention to this, Bayazitoglu et al. [36] concluded that triangular and square pin-fin arrangements showcased the highest values of Nusselt number when compared to other options, indicating superior thermal performance. However, triangular and square pin fins also induce the largest pressure drop within the microchannel which would result in high pumping power required. To investigate the potential of enhancing the heat transfer performance within square pin fins, Huang et al. [37] studied the effect of varying attack angles upon a square pin-fin, ranging from 0 to 45 degrees. It was found that increasing the attack angle up to 30 degrees will greatly increase thermal performance and generally causes negligible flow resistance due to the boundary of the square pin-fins being in-line with the streamline of the flow, overall resulting in an enhanced convection effect. Bhandari and Prajapati [25] had compared pin-fin microchannel heat sinks consisting of different pin fin heights, utilizing water coolant of laminar flow with a constant heat flux within the range of 75-150 kW/m^2 being exerted to the microchannel. It was concluded that utilizing a pin-fin height that is four-fifths of the overall flow height will result in the best thermal performance within the heat sink where increasing or decreasing the fin height will worsen the heat dissipation effects. With appropriate clearance given, there is an enhanced effect on the recirculation and mixing of the coolant in the open spaces between the pin fins, enhancing heat transfer.

With an extensive range of studies conducted towards improving the performance of the microchannel heat sink, there has been a significant void of studies that have focused on the subsequent effects on the solid substrate due to thermal stresses and deformations.

The microchannel heat sink material is exposed to expansions and contractions of the solid substrate due to the difference in the temperatures along and across the heat sink. The mechanism of these expansions and contractions acting upon the microchannel results in the formation of thermal stresses. These deformations and thermal stresses may result in structural damage to the microchannel, significantly hampering its ability to dissipate heat effectively

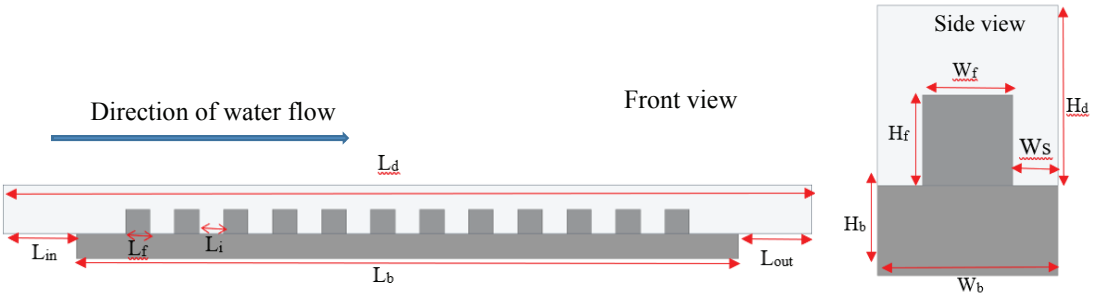

Figure 1. Schematic diagram of the physical model.

and accelerating mean time to failure. Due to the lack of such important investigations, a parametric study is conducted in this article. The parameters to be considered within the static structural analysis will be the Reynolds number, heat flux applied to the bottom of the microchannel and the type of material to be utilized within the solid substrate. Following the study conducted by Bhandari and Prajapati [25], a rectangular cross-section microchannel consisting of a row of 12 square pin fins will be considered as shown in Figure 1 and Table 1. A constant heat flux is applied to the bottom of the microchannel where the solid substrate will be cooled by water coolant.

Table 1. Dimensional parameters of the pin-fin microchannel

	Notation	Value(mm)
Length of fin	Lf	1
Foot print area of fins	Lf x Wf	1x1
Length of duct	Ld	30
Length of base	Lb	27
Length in between fins	Lc	1
Length of inlet	Lin	1.5
Height of duct	Hd	2
Height of fins	Hf	1
Base thickness	Hb	1
Base width/Duct width	Wb	2
Fin width	Wf	1
Distance between fins and side walls	Ws	0.5

MATHEMATICAL MODEL

The governing equations for the heat and fluid flow are the continuity, momentum and energy equations which derives from the mass, momentum and energy conservations respectively. The fluid flow is assumed incompressible Newtonian fluid in the laminar flow conditions. Viscous heating along with the effect of gravity and radiation heat transfer are ignored. Therefore, the governing equations can be written as follows:

$$\frac{\partial u}{\partial x}+\frac{\partial v}{\partial y}+\frac{\partial w}{\partial z}=0 \tag{1}$$

$$\rho\left(u\frac{\partial u}{\partial x}+v\frac{\partial u}{\partial y}+w\frac{\partial u}{\partial z}\right)=-\frac{\partial P}{\partial x}+\mu\left(\frac{\partial^2 u}{\partial x^2}+\frac{\partial^2 u}{\partial y^2}+\frac{\partial^2 u}{\partial z^2}\right) \tag{2}$$

$$\rho\left(u\frac{\partial v}{\partial x}+v\frac{\partial v}{\partial y}+w\frac{\partial v}{\partial z}\right)=-\frac{\partial P}{\partial x}+\mu\left(\frac{\partial^2 v}{\partial x^2}+\frac{\partial^2 v}{\partial y^2}+\frac{\partial^2 v}{\partial z^2}\right) \tag{3}$$

$$\rho\left(u\frac{\partial w}{\partial x}+v\frac{\partial w}{\partial y}+w\frac{\partial w}{\partial z}\right)=-\frac{\partial P}{\partial x}+\mu\left(\frac{\partial^2 w}{\partial x^2}+\frac{\partial^2 w}{\partial y^2}+\frac{\partial^2 w}{\partial z^2}\right) \tag{4}$$

$$\rho c_p\left(u\frac{\partial T}{\partial x}+v\frac{\partial T}{\partial y}+w\frac{\partial T}{\partial z}\right)=k\left(\frac{\partial^2 T}{\partial x^2}+\frac{\partial^2 T}{\partial y^2}+\frac{\partial^2 T}{\partial z^2}\right) \tag{5}$$

where the velocity component u, v, and w are in the x, y, and z directions respectively, T is the fluid temperature, ρ is the density, μ is the dynamic viscosity, P is the pressure, c_p is the specific heat at constant pressure and k is the thermal conductivity.

The steady state conduction within the solid substrate is governed by the following equations:

$$\frac{\partial^2 T_s}{\partial x^2}+\frac{\partial^2 T_s}{\partial y^2}+\frac{\partial^2 T_s}{\partial z^2}=0 \tag{6}$$

where the subscript s represents the solid. No slip boundary condition was applied to the solid surfaces. For the interface solid fluid surfaces, the coupled thermal boundary condition is implemented as:

$$T_s=T \tag{7a}$$

$$k_s\frac{\partial T_s}{\partial n}=k\frac{\partial T}{\partial n} \tag{7b}$$

where n is the normal direction. Water is used as the cooling fluid with constant properties as: dynamic viscosity, μ = 0.001003 kg/ms, density, ρ = 1000 kg/m^3, and thermal conductivity k = 4.18 kJ/kgK.

Constant inlet velocity and temperature are imposed at the inlet section. The inlet velocity is calculated from the

specified Reynolds number, which is defined based on the hydraulic diameter as: $Re = \rho u_{in} D_h / \mu$. The cooling performance of the heat sink is evaluated using the average Nusselt number, which is defined as: $Nu = hD_h/k$. The average heat transfer coefficient h is calculated from the results of the thermal field.

The temperature field produced from the thermal analysis is generating thermal stresses and deformations. The thermal stresses are governed by the following equations [38]:

$$\frac{\partial \sigma_x}{\partial x} + \frac{\partial \tau_{xy}}{\partial y} + \frac{\partial \tau_{xz}}{\partial z} = 0 \tag{8}$$

$$\frac{\partial \tau_{xy}}{\partial x} + \frac{\partial \sigma_y}{\partial y} + \frac{\partial \tau_{yz}}{\partial z} = 0 \tag{9}$$

$$\frac{\partial \tau_{xz}}{\partial x} + \frac{\partial \tau_{yz}}{\partial y} + \frac{\partial \sigma_z}{\partial z} = 0 \tag{10}$$

where σ is the normal stress, τ is the shear stress. The relationship between the stresses and the resultant strains are given by Hooke's law, which can be written as:

$$\sigma_x = \frac{E}{(1+v)}(\varepsilon_x - \varepsilon_T) \tag{11}$$

$$\sigma_y = \frac{E}{(1+v)}(\varepsilon_y - \varepsilon_T) \tag{12}$$

$$\sigma_z = \frac{E}{(1+v)}(\varepsilon_y - \varepsilon_T) \tag{13}$$

$$\tau_{xy} = \frac{E}{2(1+v)}\gamma_{xy} \tag{14}$$

$$\tau_{xz} = \frac{E}{2(1+v)}\gamma_{xz} \tag{15}$$

$$\tau_{yz} = \frac{E}{2(1+v)}\gamma_{yz} \tag{16}$$

where E is the Young's Modulus, v is the Poisson's ratio. ε is the normal strain, γ is the shear strain. The strain leading to the deformation formed can be directly related to the thermal expansion coefficient of the solid substrate by the following equation:

$$\varepsilon_T = \alpha(T_s - T_{ref}) \tag{17}$$

where ε_T is the thermal strain, α is the thermal expansion coefficient, T_s is the temperature of the solid substrate and T_{ref} is the reference temperature at zero stress. The strain components can be written in terms of displacements as follows:

$$\varepsilon_x = \frac{\partial s_x}{\partial x};\ \varepsilon_y = \frac{\partial s_y}{\partial y};\ \varepsilon_z = \frac{\partial s_z}{\partial z};\ \gamma_{xy} = \frac{\partial s_x}{\partial y} + \frac{\partial s_y}{\partial x};\ \gamma_{xz} = \frac{\partial s_x}{\partial z} + \frac{\partial s_z}{\partial x};\ \gamma_{yz} = \frac{\partial s_y}{\partial z} + \frac{\partial s_z}{\partial y} \tag{18}$$

where s represents the displacement of the material due to thermal stresses. The equivalent stresses (or von Mises stresses) are usually used in the static structural analysis, which can be expressed by the following equation:

$$\sigma_{VM} = \sqrt{\sigma_x{}^2 + \sigma_y{}^2 + \sigma_z{}^2 - \sigma_x\sigma_y - \sigma_x\sigma_z - \sigma_z\sigma_y + 3[(\tau_{xy})^2 + (\tau_{xz})^2 + (\tau_{zy})^2]} \tag{19}$$

NUMERICAL SOLUTION METHOD

The numerical solution of the mathematical models is carried out using ANSYS R2 2022 software. FLUENT software (which is a part of ANSYS) [39] is used to solve the mathematical model for heat and fluid flow defined in the equations (1)-(7). For the solid mechanics and stress analysis, the Static Structural software (which is a part of ANSYS) is used to solve the governing equations for thermal stress formations and deformation defined in the equations (8)-(19).

The numerical solution produced for the fluid flow and heat transfer is based on finite volume method whereas the structural analysis will utilize the finite element method. The geometry is divided into multiple various two-dimensional elements for the surface area and three-dimensional segments for the volume. Due to the relatively simple geometry, a structured quadrilateral mesh was adopted for a majority of the grid with an average element sizing of 1.3×10^{-4} m. Figure 2 shows the top view of the mesh geometry of part of the channel and the fins.

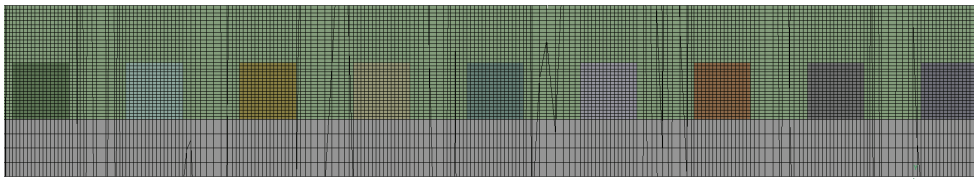

Figure 2. Top view of the mesh geometry.

Table 2. Properties of the solid materials

Material	Copper	Aluminum	Steel	Titanium
Density, ρ (kg/m^3)	8933	2719	8030	4850
Thermal conductivity, k (W/m.K)	401	202.4	16.27	7.44
Specific heat, cp (J/kg.K)	385	871	502.48	544.25
Youngs modulus, E (Pa)	1.10E+11	7.10E+10	2.00E+11	9.60E+10
Poissons ratio, ν	0.34	0.33	0.3	0.36
Bulk modulus, K (Pa)	1.15E+11	6.96E+10	1.67E+11	1.14E+11
Shear modulus, G (Pa)	4.10E+10	2.67E+10	7.69E+10	3.53E+10
Thermal expansion coefficient, α (1/°C)	1.8E-05	2.3E-05	1.20E-05	9.40E-06

The fluid used in this study is water where its properties are considered to be varying dependently upon the fluid temperature [40]. The governing equations for the properties of the water are as follows:

$$\rho = 765.33 + 1.8142T - 0.0035T^2 \quad (20a)$$

$$k = -0.5752 + (6.79 \times 10^{-3})T - (8.151 \times 10^{-6})T^2 \quad (20b)$$

$$c_p = 28070 - 281.7T + 1.25T^2 - (2.48 \times 10^{-3})T^3 + (1.857 \times 10^{-6})T^4 \quad (20c)$$

$$\mu = (9.67 \times 10^{-2}) - (8.207 \times 10^{-4})T + (2.344 \times 10^{-6})T^2 + (2.244 \times 10^{-9})T^3 \quad (20d)$$

The solid component of the microchannel heat sink, which includes the base and the fins, are to be made up of any of the following materials: Copper Aluminium, Steel, and Titanium. The thermal and structural properties of these solid materials are listed in Table 2 [36].

The water enters the channel from the left side with constant velocity and temperature and exit from the right side to the atmospheric pressure as shown in Figure 1. The bottom surface of the channel is subjected to constant heat flux. The coupled boundary condition (defined in equation (7)) is imposed to the fin surfaces and the surface in-between the fins. The symmetry boundary condition is imposed on the side surfaces of the channel, where the gradient of all the dependent variables are set to zero on these surfaces.

In the solution method, SIMPLE algorithm [39] is used for pressure-velocity coupling with second order upwind scheme for solving the momentum and energy equations.

The resulting thermal field and fluid flow are then exported to Static Structural model to undergo structural analysis in efforts to investigate the thermal stresses and deformations. In the structural analysis the fluid section is to be suppressed within the structural analysis and boundary conditions are applied. Zero displacements are set on the bottom of the base, symmetry surfaces and inlet/outlet surface in all directions. These boundary conditions are established in order to accurately approximate the constraints of a microchannel heat sink within the actual operations.

RESULTS AND DISCUSSION

For validation purposes, the results of the present model using various mesh sizing are compared with the results of Bhandari and Prajapati [25] for the average Nusselt number (Nu) at various Reynolds numbers (Re). Note that the study by Bhandari and Prajapati [25] utilized a pin microchannel geometry with multiple rows of pin-fins rather than a singular row of pin fins. For the validation study, the present model, copper is used as the material for the solid substrate with a constant heat flux of 150 kW/m^2 applied to the bottom of the microchannel. The results of the comparison are presented in Table 3. For verification of the present model, the grid independent study is conducted using coarse mesh

Table 3. Comparison of the average Nusselt number values

Re	Bhandari and Prajapati [25]	Present Results		
		31324 elements (Coarse)	342154 elements (Moderated)	510456 elements (Fine)
200	15.11	14.66	14.74	14.74
400	20.47	18.43	19.29	19.28
600	24.56	21.37	23.59	23.56
800	28.11	23.94	28.17	28.12

with 31324 elements, moderated size mesh with 342154 element, and fine mesh with 510456 elements. The present results listed in Table 3 were generated for the same model and boundary condition but using 3 different meshes. The differences between the values of the Nusselt number calculated using the moderated size mesh and the fine mesh are negligible.

It can be concluded from Table 3 that the results for Nusselt number from the present solution are within a small margin of difference to the results presented by Bhandari and Prajapati [25] (<10%). Therefore, the present results can be considered as valid results and grid independent simulations. The moderated size mesh is used to generate the results for the parametric study.

The details of the velocity and temperature contours for the validation case (Cupper heat sink subjected to a heat flux of 150 kW/m^2) study are presented in Figure 3 and 4 respectively.

The velocity contours presented in Figure 3, show that the average velocity profile increases with increasing Reynolds number. The velocity reaches its highest magnitude in the region directly above the pin-fins due to the smaller flow area with constant mass flow rate (due to the constant velocity condition boundary condition applied) at the inlet.

Figure 4 shows the temperature contours, in which it can be observed that the average temperature profile of the pin-fins decreases in temperature with increasing Reynolds Number. The same trend can be observed within the fluid upon leaving the last fin in the heat sink. This trend is due to the increase of Reynolds number (as a result of the increasing flow velocity) allows for more efficient and intense transport/mixing of the fluid. This allows for an increase of the convective heat transfer effect within the fluid hence allows better cooling of the solid pin-fin arrays.

The calculated values of the average Nusselt number at various values of Reynolds number and heat fluxes are

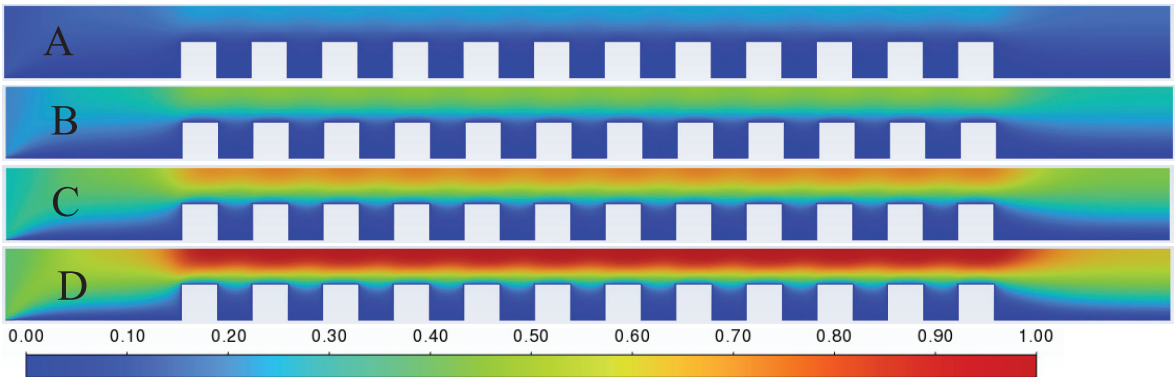

Figure 3. Velocity contours (m/s) with heat flux of 150 kW/m^2 and (A) Re=200, (B) Re=400, (C) Re=600, (D) Re=800.

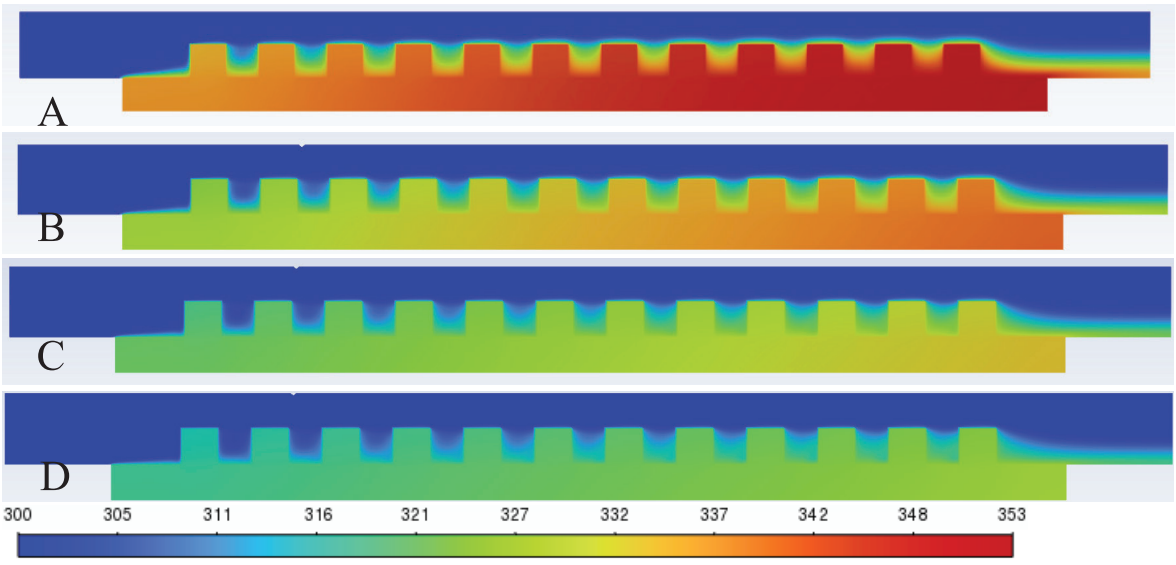

Figure 4. Temperature contours (K) with heat flux of 150 kW/m^2 and (A) Re=200, (B) Re=400, (C) Re=600, (D) Re=800.

presented in Figure 5. It can be observed from Figure 5, the Nusselt number increases with increasing Reynolds number. This is due to the increasing overall heat transfer coefficient between the fluid and solid section within the microchannel heat sink as the Reynolds Number increases. Figure 5 shows also that varying the heat flux is not significantly affect the resulting Nusselt number at a constant Reynolds number (difference of < 5%). This is due to the heat transfer capability (heat transfer coefficient) of the microchannel heat sink remaining constant throughout no matter the amount of heat flux applied as the temperature rise within the system would vary accordingly and therefore the Nusselt number will not change significantly.

Figure 6 shows the effect of changing the solid material of the microchannel on the variation of Nusselt number against Reynolds number for fixed value of heat flux of 150 kW/m^2. The calculated Nusselt numbers show the highest for the cases which utilizing the high conductive materials (Copper and Aluminium). This is due to values of the thermal conductivity of the material (presented in Table 2), where the higher the thermal conductivity, leads to the higher value of the heat transfer coefficient and Nusselt number.

For the same case study geometry and dimensions, which is used for the validation, the thermal field obtained

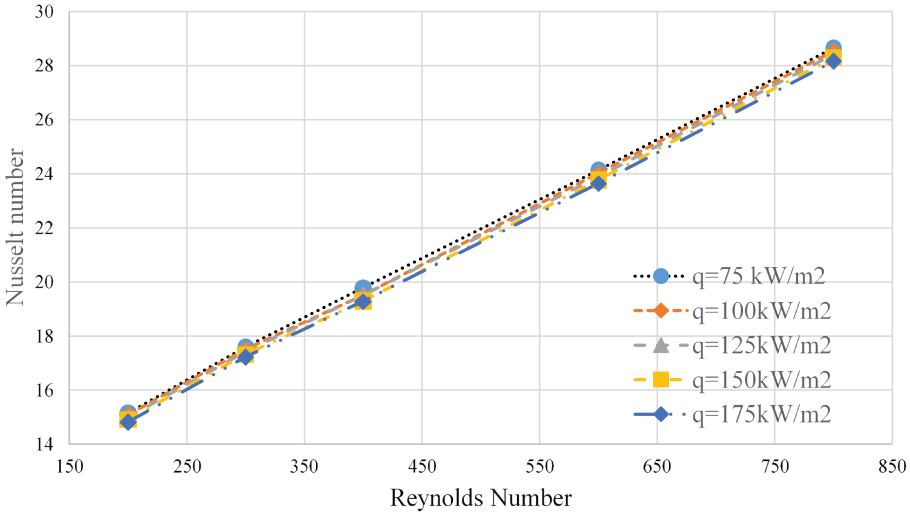

Figure 5. Variation of Nusselt number with various Reynolds Numbers and heat fluxes for Copper microchannel.

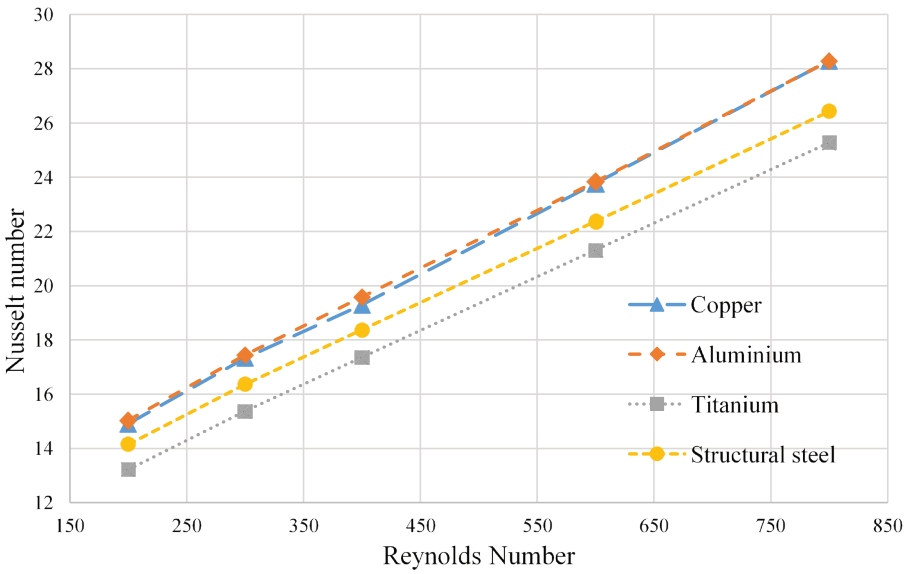

Figure 6. Variation of the Nusselt number with Reynolds Number and material of the microchannel for fixed value of heat flux of 150 kW/m^2.

in the computational fluid dynamics (CFD) analysis is exported and communicated to the structural analysis.

Figure 7 shows the thermal equivalent stress contours in the steel solid substrate microchannel heat sink, which are obtained from the solution of the static solid mechanics model defined in equations (8) to (19). By observing the contour in Figure 7, it can be seen that the higher values of thermal stresses are concentrated within the base section of the microchannel where these base stresses will peak in the area surrounding the pin fins. The stresses towards the top of the pin fins are generally low. This is due to the pin fins experiencing the maximum cooling effect through convection with the fluid flow. This results in the pin fins having a significantly higher heat transfer compared with the base section therefore hampering the formation of significant thermal stresses. However, the bottom of the pin fins experiences less direct exposure to fluid flow (mostly experiencing recirculated flow), therefore the heat transfer occurring at the bottom of the pin fins is less than the top of the pin fin. This leads to the thermal stresses at the bottom of the pin fin are significantly higher than the rest of the pin fin.

It is important to note that the point position where maximum thermal stresses will be experienced in the solid substrate will be within the heat dissipation area surrounding the last pin-fin before the outlet as shown in Figure 7. This is due to the fluid is heated while flowing through the channel and reaching its highest temperature point when approaching the outlet section. Both the fluid and solid sections near the outlet are at relatively high temperatures with not much heat transfer occurring between the two sections therefore the solid section will experience maximum thermal load at the outlet section causing the subsequent thermal stress.

The maximum thermal stresses experienced within the microchannel heat sink decreases with increasing Reynolds number (at constant heat flux) as shown in Figure 8 for copper heat sink. As Reynolds number increases, the heat transfer coefficient increases leading to an enhanced cooling effect upon the solid substrate, resulting in a decrease of the thermal load within the heat dissipation interface.

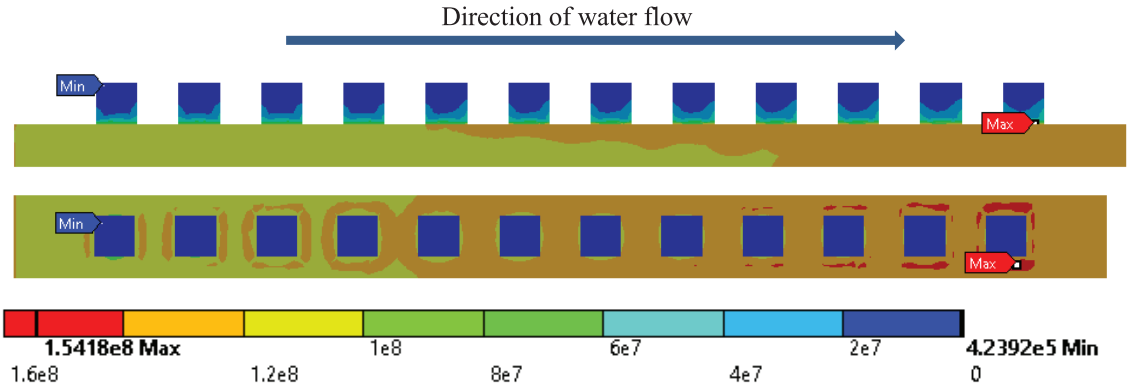

Figure 7. Side view (Top) and top view (bottom) of the thermal equivalent stress contour of steel solid substrate microchannel heat sink at Re=400 and q=150 kW/m^2.

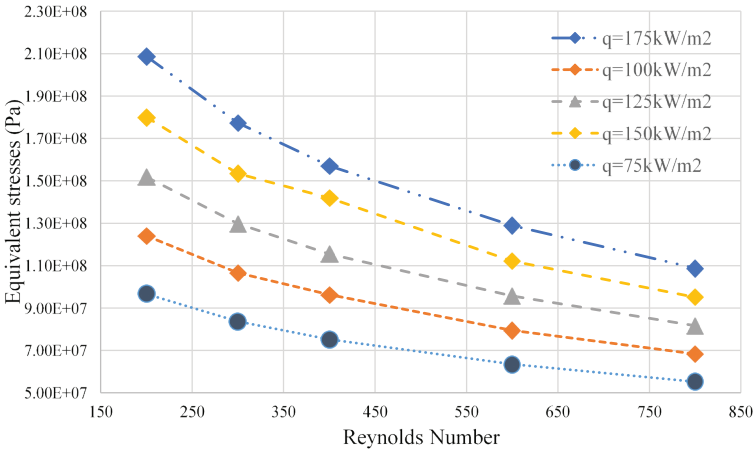

Figure 8. Variation of maximum equivalent thermal stresses against the Reynolds numbers of the fluid flow at various heat fluxes applied on the copper substrate.

In an opposite sense, again referring to Figure 8, the maximum thermal stresses experienced within the copper microchannel heat sink will increase as the heat flux applied increases (at constant Reynolds number). Since overall heat transfer characteristic of the microchannel heat sink does not increase with the heat flux applied therefore the cooling effect upon the solid section will not vary, resulting in the residual thermal load within the microchannel heat sink to increase with the heat flux. Overall, this will lead to increasing thermal stresses to form within the solid substrate.

The results of the maximum equivalent thermal stresses generated within different materials of the solid substrate at various values of Reynolds Number is presented in Figure 9 for a fixed heat flux of 150 kW/m^2. It can be observed that the maximum thermal stresses being experienced will be the highest in the structural steel substrate followed by copper then aluminium and finally titanium. This is due to the Youngs modulus of the materials dictating the behaviour of the thermal stresses produced which can be verified by referring to the structural properties for the materials. Similar results were presented by Saeid [41] for the case of jet impingement cooling of a solid block.

The total deformations are calculated for Aluminium microchannel subjected to heat flux 150 kW/m^2 and cooled with water flow at Re = 400 and their contour plots are presented in Figure 10. It can be seen in Figure 10 that the greater values of deformation within the microchannel heat sink is concentrated within the mid-section of the microchannel heat sink with minimal deformation occurring along the inlet and outlet section of the heat sink. It is noted that at each pin fin, the deformations will peak at the top of the pin-fin. The maximum deformation being experienced in heat sink is at the 5th pin fin away from the outlet, roughly in the midsection along the microchannel fluid flow. This is due to the zero displacement conditions applied to the outer walls of the solid section within the present structural model.

The results of the maximum deformation produced within the copper pin-fin microchannel against Reynolds number at varying heat fluxes are presented in Figure 11. It can be observed that the maximum deformation produced within the pin-fin microchannel will follow the same trends as the thermal stresses produced. The maximum deformation produced decreases with increasing Reynolds

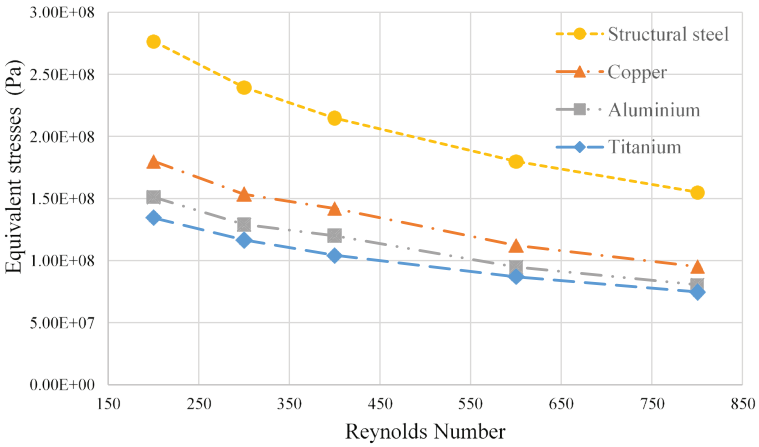

Figure 9. Variation of maximum equivalent thermal stresses against the Reynolds numbers with various solid materials and constant heat flux = 150 kW/m^2.

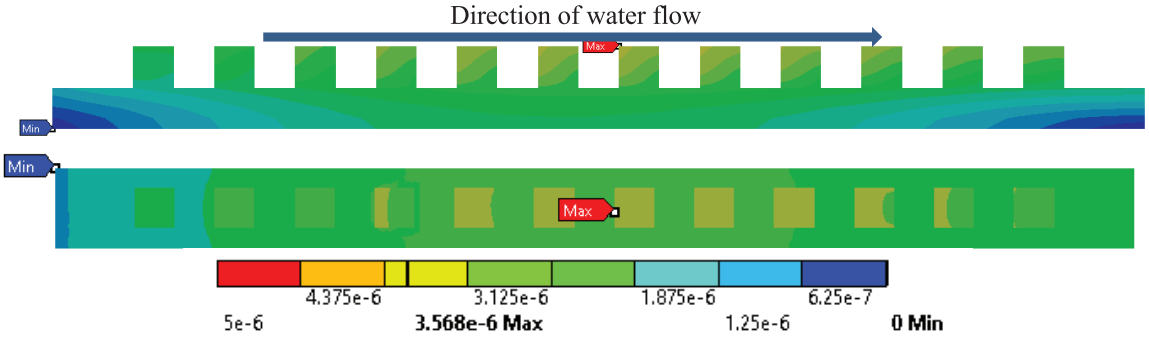

Figure 10. Total deformation contour of Aluminium solid substrate at Re=400, q=150 kW/m^2.

number (at constant heat flux and solid substrate material) and increases as applied heat flux increases (at constant Reynolds number and solid substrate material).

However, the structural properties of the solid substrate are important factors affecting the deformation produced within the solid material as shown in Figure 12. The results presented in Figure 12 for a fixed heat flux of 150 kW/m², show that the highest maximum deformation being experienced is in the structural steel substrate followed by aluminium then copper and finally titanium. The main reason for this variation is due to the difference in the coefficient of thermal expansion of the materials. Once again, upon viewing the list of material structural properties in Table 2, it can be observed that aluminium possesses the highest coefficient of thermal expansion. The higher thermal expansion coefficient will allow for proportionately greater deformation as a result of a fixed thermal load. However, it is to be noted that structural steel has a greater maximum deformation induced in comparison to copper which defers from the trend seeing as copper has a higher thermal expansion coefficient (1.8E-05 /°C) than structural steel (1.2E-05 /°C). This is a result of the structural steel substrate possessing a much higher thermal stress profile than copper, as shown in Figure 9. Therefore, the results presented in Figure 12 for total deformation are for the combined effects of thermal stresses and coefficient of thermal expansion.

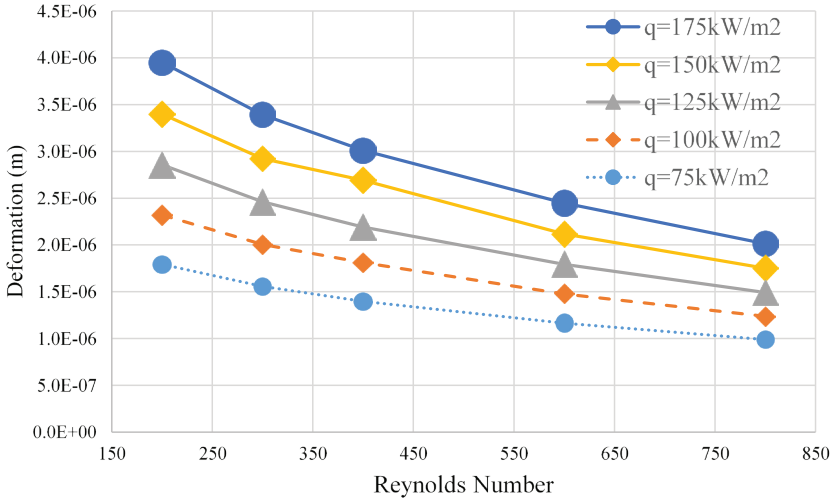

Figure 11. Variation of maximum total deformations against Reynolds Number at varying heat fluxes applied on the copper substrate.

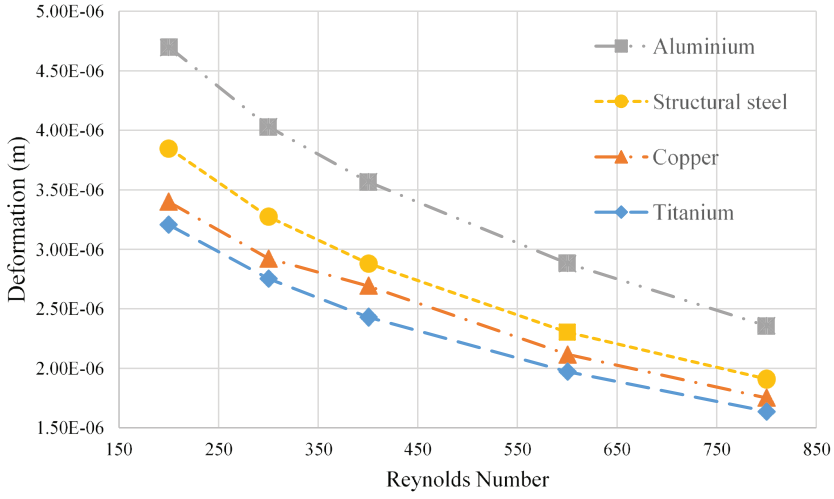

Figure 12. Variation of maximum total deformations produced against Reynolds Number with various solid materials and constant heat flux = 150 kW/m².

CONCLUSION

The present study focused on investigating the effect of fluid flow and heat transfer properties in microchannel heat sink with square fins upon the heat dissipation and the generated thermal stresses and deformations within the solid section. The microchannel heat sink is utilizing water as its coolant with temperature dependent properties. The parameters considered in the present study are: (1) Reynolds number in the laminar regime (200-800); (2) heat fluxes applied at the bottom surface of the microchannel (75-175kW/m^2); (3) the material of the microchannel and the fins (Copper, Aluminium, Structural Steel, Titanium alloy).

The results show that the Nusselt number rises with increasing Reynolds number and increasing thermal conductivity of the solid section while remaining generally unaffected by varying heat fluxes applied. Higher values of equivalent thermal stress are concentrated within the base section of the microchannel, reaching its peak within the heat dissipation area surrounding the last pin-fin before the reaching the outlet section.

The present numerical results show that the thermal stresses at the bottom of the pin fin are significantly higher than the rest of the pin fin where along with this, the thermal stresses are concentrated within the sides of the pin fins. Therefore, the contact areas of the pin fins with the base plate have high possibility of failure if the created thermal stresses exceed the material's ultimate tensile strength. The thermal stresses experienced within the microchannel heat sink will decrease with increasing Reynolds number, increase with increasing heat flux applied and increases with increasing Youngs Modulus of the material utilized.

The total deformation within the microchannel heat sink will be much higher within the general mid-section of the microchannel heat sink, perpendicular to the fluid flow. The total deformations are more concentrated within the pin fins rather than the base section. The deformations produced would decrease with increasing Reynolds number, increase as either the applied heat flux and/or the coefficient of thermal expansion increases. The present study can be extended to consider various geometry of the fins in the microchannel heat sink used in the cooling of the electronics.

AUTHORSHIP CONTRIBUTIONS

Authors equally contributed to this work.

DATA AVAILABILITY STATEMENT

The authors confirm that the data that supports the findings of this study are available within the article. Raw data that support the finding of this study are available from the corresponding author, upon reasonable request.

CONFLICT OF INTEREST

The author declared no potential conflicts of interest with respect to the research, authorship, and/or publication of this article.

ETHICS

There are no ethical issues with the publication of this manuscript.

REFERENCES

[1] Guo ZY. Frontier of heat transfer - microscale heat transfer. Adv Mech 2000;30:1−6.

[2] Singh PK, Lee YJ, Lee PS. Integrated thermal management techniques for high power electronic devices. Appl Therm Eng 2015;81:325−336.

[3] Zunaid M, Jindal A, Gakhar D, Sinha A. Numerical study of pressure drop and heat transfer in a straight rectangular and semi cylindrical projections microchannel heat sink. J Therm Eng 2017;3:1453−1465. [CrossRef]

[4] Kelly KW, Marques C. Fabrication and performance of a pin fin micro heat exchanger. ASME J Heat Transfer 2004;126:434−444. [CrossRef]

[5] Ortega A, Kim D, Kim SJ. Compact modeling of fluid flow and heat transfer in pin fin heat sinks. ASME J Heat Transfer 2004;48:342−350. [CrossRef]

[6] Sparrow EM, Grannis VB. Pressure drop characteristics of heat exchangers consisting of arrays of diamond-shaped pin fins. Int J Heat Mass Transfer 1991;34:589−600. [CrossRef]

[7] Liao G, Wang X, Li J, Zhang F. A numerical comparison of thermal performance of in-line pin-fins in a wedge duct with three kinds of coolant. Int J Heat Mass Transfer 2014;77:1033−1042. [CrossRef]

[8] Thoble KA, Lawson SA, Thrift AA. Heat transfer from multiple arrays of low aspect ratio pin fins. Int J Heat Mass Transfer 2011;54:4099−4109. [CrossRef]

[9] Schnei B, Kuo CJ, Peles Y, Kosar A. Forced convective heat transfer across a pin fin micro heat sink. Int J Heat Mass Transfer 2005;48:3615−3627. [CrossRef]

[10] Prasher RS, Dirner J, Chang J, Myers A, Chau D, He D, Prstic S. Nusselt number and friction factor of staggered array of low aspect ratio micro-pin-fins under cross flow for water as fluid. ASME J Heat Transfer. 2007;129:141−153. [CrossRef]

[11] Siu-Ho A, Qu W. Liquid single-phase flow in an array of micro-pin-fins - part I: heat transfer characteristics. ASME J Heat Transfer 2008;130. [CrossRef]

[12] Kosar A, Peles Y. Thermal-hydraulic performance of MEMS-based pin fin heat sink. ASME J Heat Transfer 2006;128:121−131. [CrossRef]

[13] Peles Y, Kosar A. Micro scale pin fin heat sinks - parametric performance evaluation study. IEEE Trans Components Packaging Technol 2007;30:855−865. [CrossRef]

[14] Liu MH, Liu D, Xu S, Chen YL. Experimental study on liquid flow and heat transfer in micro square pin fin heat sink. Int J Heat Mass Transfer 2011;54:5602−5611. [CrossRef]
[15] Gunnasegaran P, Mohammed H, Shuaib N, Saidur R. The effect of geometrical parameters on heat transfer characteristics of microchannels heat sink with different shapes. Int Commun Heat Mass Transfer 2010;37:1078−1086. [CrossRef]
[16] Kewalramani GV, Hedau G, Saha SK, Agraw A. Study of laminar single phase frictional factor and Nusselt number in In-line micro pin-fin heat sink for electronic cooling applications. Int J Heat Mass Transfer 2019;138:796−808. [CrossRef]
[17] Cheng Y. Numerical simulation of stacked microchannel heat sink with mixing-enhanced passive structure. Int Comm Heat Mass Transf 2007;34:295−303. [CrossRef]
[18] Xie G, Shen H, Wang CC, Zhang Y. Comparative study for convective heat transfer of counter-flow wavy double-layer microchannel heat sinks in staggered arrangement. Appl Therm Eng 2018;137:228−237. [CrossRef]
[19] Wang TH, Leng C, Wang XD. An improved design of double-layered microchannel heat sink with truncated top channels. Appl Therm Eng 2015;79:54−62. [CrossRef]
[20] Ding G, Wang G, Niu D, Zhao X, Wang Y, Xie F, Wang G. Experimental and numerical investigation of a microchannel heat sink (MCHS) with micro-scale ribs and grooves for chip cooling. Appl Therm Eng 2015;85:61−70. [CrossRef]
[21] Kamaruzaman N, Sidik NA, Ghani IA. Hydrothermal performance of microchannel heat sink: The effect of channel design. Int J Heat Mass Transf 2017;107:21−44. [CrossRef]
[22] Sun H, Liu X, Zhang M, Wang Z, Chen J. Numerical analysis of fluid flow and heat transfer in micro-channel heat sinks with double-layered complex structure. Micromachines 2020;11:146. [CrossRef]
[23] Cheng W, Nian Y, Zhao R, Pan Y. Study on the flow and heat transfer characteristics of pin-fin manifold microchannel heat sink. Int J Heat Mass Transf 2021;183. [CrossRef]
[24] Wang H, Xia G, Chai L. Parametric study on thermal and hydraulic characteristics of laminar flow in microchannel heat sink with fan-shaped ribs on sidewalls - Part 2: Pressure drop. Int J Heat Mass Transf 2016;97:1081−1090. [CrossRef]
[25] Bhandari P, Prajapati YK. Thermal performance of open microchannel heat sink with variable pin fin height. Int J Thermal Sci 2021;159. [CrossRef]
[26] Park C, Ali H, Abbas A, Khan M, Cheema T, Rehman MU. Parametric evaluation of a hydrofoil-shaped sidewall rib-employed microchannel heat sink with and without nano-encapsulated phase change material slurry as coolant. Appl Therm Eng 2020;178. [CrossRef]
[27] Grande WJ, Kandlikar SG. Evaluation of single phase flow in microchannels for high heat flux chip cooling-thermohydraulic performance enhancement and fabrication technology. In: ASME 2004 2nd International Conference on Microchannels and Minichannels. Rochester, NY: 2004. [CrossRef]
[28] Luo Y, Wang H, Bai P, Cai R, Tang Y, Chen X, Li S, Wu G, Zhou G. A hybrid vapor chamber heat sink incorporating a vapor chamber and liquid cooling channel with outstanding thermal performance and hydraulic characteristics. Energy Convers Manag 2021;244. [CrossRef]
[29] Park CW, Ambreen T, Saleem A. Pin-fin shape-dependent heat transfer and fluid flow characteristics of water- and nanofluid-cooled micropin-fin heat sinks: Square; circular and triangular fin cross-sections. Appl Therm Eng 2019;158. [CrossRef]
[30] Mohammadian SK, Zhang Y. Analysis of nanofluid effects on thermoelectric cooling by micro-pin-fin heat exchangers. Appl Therm Eng 2014;70:282−290. [CrossRef]
[31] Sartipzadeh O, Khoshvaght-Aliabadi M, Ahmadian E. Effects of different pin-fin interruptions on performance of a nanofluid-cooled zigzag miniature heat sink (MHS). Int Comm Heat Mass Transf 2017;81:19−27. [CrossRef]
[32] Arshad W, Ali H. Thermal performance investigation of staggered and inline pin fin heat sinks using water-based rutile and anatase TiO2 nanofluids. Energy Convers Manag 2015;106:793−803. [CrossRef]
[33] Kaya H, Ekiciler R, Arslan K. CFD analysis of laminar forced convective heat transfer for TiO2/water nanofluid in a semi-circular cross-sectioned micro-channel. J Therm Eng 2019;5:123−137. [CrossRef]
[34] Ronge BP, Jadhav SV, Pawar PM. Effect of pin-fin geometry on microchannel performance. Chem Prod Process Model 2018;14. [CrossRef]
[35] Saha SK, Kewalramani GV, Agrawal A. Modeling of microchannel heat sinks for electronic cooling applications using volume averaging approach. Int J Heat Mass Transf 2017;115:395−409. [CrossRef]
[36] Bayazitoglu Y, Tullius TK, Tullius JF. Optimization of short micro pin fins in minichannels. Int J Heat Mass Transf 2012;55:3921−3932. [CrossRef]
[37] Huang Z, Zhao J, Huang S, Gong L. Numerical study and optimizing on micro square pin-fin heat sink for electronic cooling. Appl Therm Eng 2016;93:1347−1359. [CrossRef]
[38] Dechaumphai P, Sucharitpwatskul S, Sedthawat S. Heat transfer and thermal stress analysis. In: Finite Element Analysis with ANSYS Workbench. Oxford: Alpha Science International Ltd.; 2018. pp. 166−190.
[39] ANSYS FLUENT User's Guide. Canonsburg, PA: ANSYS Inc.; 2013. pp. 15317.

[40] Cengel YA, Cimbala JM. Introduction to computational fluid dynamics. In: Fluid Mechanics: Fundamentals and Applications. McGraw-Hill: 2006. pp. 817−833.

[41] Saeid NH. Thermal stress analysis of jet impingement cooling of a solid block. Heat Transf Eng 2023;44:87−101. [CrossRef]